1   **Natural iron fertilisation stimulates a carbonate counter pump in the**

2   **Polar Frontal Zone**

3

4   **Iron (Fe) fertilisation of Southern Ocean high nutrient low chlorophyll (HNLC)**

5   **waters increases biological productivity[1-3] and carbon export to subsurface[2, 3]**

6   **and deep waters[3-5]. The supply of Fe has been widely discussed as a mechanism**

7   **to explain glacial atmospheric carbon dioxide (CO_2) fluctuations[6-8] and a**

8   **potential strategy to mitigate climate warming. However, deep-ocean storage of**

9   **atmospheric CO_2 depends on the <mark>rain ratio (organic to inorganic carbon)</mark>**

10   **exported from the surface ocean[9] and the response of major planktonic calcifiers**

11   **to Fe enrichment is unknown. <mark>Here we show from particle analysis of sediment</mark>**

12   **<mark>trap samples deployed in the polar frontal Zone that natural iron supply leads to</mark>**

13   **<mark>excess (Fe-fertilized minus HNLC) particulate inorganic carbon (PIC) fluxes</mark>**

14   **<mark>greater than the corresponding excess organic carbon fluxes.</mark> Resulting rain**

15   **ratios are <1; a unique occurrence south of the Subantarctic Front. Our**

16   **conservative estimates indicate that PIC fluxes reduce deep-ocean CO_2 storage**

17   **by ~19% (6-43%), compared to ~2.9% (1-5%) in HNLC waters. Foraminifers**

18   **are the dominant component of excess CaCO₃ fluxes (33-50%). Our data suggest**

19   **that strengthening of the Subantarctic biological carbon pump, and its**

20   **importance for CO_2 decline over the last glacial cycle, could be partially offset by**

21   **an iron fertilized carbonate counter pump.**

22

23

24

25   The biological carbon pump is the downward particulate flux of organic carbon

26   (POC) from the surface to the deep-ocean[10].   Some of the POC is not remineralized

27   in the winter mixed layer and sinks to depth driving a reduction in surface ocean

28   partial pressure of carbon dioxide (pCO_2) that is compensated by oceanic uptake of

29   atmospheric CO_2. The iron hypothesis[6] suggests that increased iron supply to the

30   nutrient-rich, but iron deficient Southern Ocean contributed towards the termination

31   of glacial periods by enhancing phytoplankton growth and the biological carbon

32   pump[7].   Recent studies of natural systems[3,4] and artificial[5] iron fertilisation

33   experiments support this idea by demonstrating enhanced POC flux well below the

34   mixed layer into the deep-ocean.

35

36   Counteracting the organic carbon pump in terms of its influence on air–sea CO_2

37   exchange is the carbonate counter pump[11]. The precipitation of $CaCO_3$ shells by

38   mainly coccolithophores, foraminifers (both calcite), and pteropods (aragonite), and

39   the resulting particulate inorganic carbon (PIC) flux from the surface ocean, causes an

40   increase in surface ocean pCO_2[12] on timescales shorter than approximately 100

41   years[13]. Due to these opposing effects, particle flux studies addressing deep-ocean

42   CO_2 sequestration need to discriminate between organic (soft-tissue) and inorganic

43   carbon, with a strong focus on a relationship formalized as the rain ratio (POC:PIC)[9].

44   Despite its obvious importance for atmospheric CO_2 the significance of $CaCO_3$ export

45   has not been explicitly considered in studies of iron fertilisation in the Southern

46   Ocean due to observations that organic carbon fluxes are primarily mediated by non-

47   calcifying phytoplankton[4-5]. However, the calcifying heterotrophic foraminifers and

48   pteropods are highly abundant in the Southern Ocean[14] and can be a dominant

49   component of PIC flux to the deep-ocean[15].

50   We carried out measurements to characterise the dynamics of PIC export from a

51   naturally iron-fertilised system in the Polar Frontal Zone (north of the Polar Front,

52   south of the Sub-Antarctic Front) and quantify the carbonate counter pump. Sediment

53   trap samples were analysed from three deployment locations. Two of the traps,

54   [+Fe]M10-N and [+Fe]M5-NE, were deployed beneath an iron-enriched [+Fe]

55   phytoplankton bloom area to the north and northeast of the Crozet Islands and the

56   third, [HNLC]M6-S, in an iron-deplete high-nutrient low chlorophyll (HNLC) zone to

57   the south[3] (Supplementary Information 1).

58

59   Our measurements quantitatively partition PIC fluxes amongst coccolithophore,

60   pteropod and foraminifer fractions, which to the best of our knowledge is the first

61   attempt to do so in the Southern Ocean (Supplementary Information 2). We place

62   particular emphasis on the species contributions of planktonic foraminifers because

63   they are a dominant component of the CaCO₃ fraction (Fig. 1a). Novel morphometric

64   particle analyses were carried out with a fully automated incident light microscope to

65   generate a continuous dataset of test-size. Manual classification and enumeration of

66   particles were combined with empirically determined CaCO₃ weights from the +Fe

67   and HNLC regions to compute the contribution of individual species to total flux

68   (Supplementary Methods).

69

70   We measured much larger annual fluxes of total, foraminifer, coccolithophore and

71   pteropod-derived PIC to the deep ocean of 7-10, 9-10, 5-8, and 63-68 times higher,

72   respectively at the +Fe sites when compared to HNLC waters (Fig. 1a, Table 1,

73   Supplementary Information 3). Previous studies from the Crozet Islands indicate

74   natural iron fertilisation enhances new production, seasonally integrated shallow

75   export, annually integrated deep-water POC flux, mega-faunal biomass, and core-top

76   organic carbon accumulation, by a factor of 2-3[3,16]. As a result of the disproportional

77   response of PIC and POC fluxes to natural iron fertilization (Table 1) in the Polar

78   Fontal Zone, deep-ocean rain ratios are reduced from 1.9 in HNLC waters to 0.6-0.8

79   at the +Fe sites (Fig 3b).

80

81   Annual carbon flux estimates from the iron-fertilized Crozet bloom were used to

82   quantify the carbonate counter pump effect in reducing CO_2 drawdown[9] to the ocean

83   interior. To achieve this we account for (i) estimates of organic carbon flux at the

84   base of the winter mixed layer (WML) (150-200m at the Crozet study site[17]), (ii)

85   deep-ocean PIC flux as a conservative estimate of WML CaCO₃ production, and (iii)

86   empirical determination of released CO_2: precipitated carbonate (Ψ)[12] ratios. The

87   principal calcifying organisms comprising the measured PIC flux in our study area

88   (Fig. 1b-d) are known to live, and by extension calcify, in the upper 50-200m of the

89   water-column[14,18,19], i.e. above the ventilation depth, where they directly contribute to

90   ocean-atmosphere CO_2 equilibrium.   Vertical profiles of dissolved inorganic carbon

91   and total alkalinity were used to calculate regional values of Ψ in the upper 200m of

92   0.77 ± 0.02 (n=24) and 0.79 ± 0.01 (n=16) at the iron-fertilized and HNLC sediment trap

93   deployment locations (Supplementary Information 4).

94

95   The resulting formulations are expressed as the reduction of CO_2 drawdown at the

96   base of the WML (Fig. 2a). Different estimates of WML POC export indicate that the

97   carbonate counter pump effect ranges from 6-43% in the [+Fe] bloom region

98   compared to 1-5% in the HNLC region. The ~15-40% reductions derived from POC

99   fluxes measured in the deep-sediment trap are considered to be the most reliable

100   estimates since POC and PIC flux budgets are integrated over identical spatial and

101   temporal scales. All of the estimates are conservative because they do not correct for

102   CaCO$_3$ dissolution[19,20] between the base of the WML and trap deployment depth

103   (Supplementary Information 5). Consequently we may have underestimated the

104   significance of an iron-fertilised carbonate counter pump in the Polar Frontal Zone.

105

106   Although there is some variability in the magnitude of our estimates, they consistently

107   demonstrate that iron-fertilisation promotes the role of the carbonate-counter pump in

108   mediating a reduction in deep-ocean CO$_2$ storage. This reflects the fact that excess

109   ([Fe] minus [HNLC]) PIC fluxes resulting from iron fertilisation are considerably

110   larger than the corresponding excess organic carbon fluxes. This is true of CaCO$_3$

111   production and flux for all calcifying plankton functional types (Fig. 1a, Table 1),

112   although the relative distribution does not change significantly (Fig 2b). Heterotrophic

113   calcifiers, notably foraminifers, account for 33-50% of annual budgets and are thus

114   the most important contributor to deep-ocean CaCO$_3$ fluxes around the Crozet

115   Plateau.

116

117   The seasonally integrated foraminifer test flux in [+Fe] waters is 0.8-1.3 x 10^{-6} tests

118   m^{-2}; a 6-10 fold increase over HNLC fluxes (Supplementary Information 3). Iron

119   supply modifies the occurrence and abundance of differently sized species (Fig. 1b-d).

120   Although *N. pachyderma* (mean size $\pm$ 1 s.d. = 166 $\pm$ 32 μm) is the dominant

121   foraminifer species at all sites, its relative abundance decreases from 68 to 36 $\pm$ 5% as

122   a result of iron fertilization (Fig 2c). There are corresponding increases in the larger

123   species *G. bulloides* (247 $\pm$ 62 μm)*, G. inflata (337 $\pm$ 93 μm), and G. crassaformis*

124   (353 $\pm$ 82 μm) in addition to *T. quinqueloba (172 $\pm$ 30* μm)*. Globorotalia inflata* and

125   *G. crassaformis* were less common and occurred primarily in association with initial

126   export events in December and January (Fig. 1b-d). Their large size, representing

127   mostly adult specimens, resulted in contributions reaching 50% of overall

128   foraminifer-PIC fluxes at those specific times, although their overall contribution to

129   annual fluxes was <10%. The fluxes of *G. bulloides* and *T. quinqueloba* were

130   sustained throughout the entire export season and their contributions to annual foram-

131   CaCO₃ budgets were approximately double under iron supply i.e. 21 ± 1.2 vs. 9 and

132   10.7 ± 4.9 vs. 2.7%, respectively. Assemblage shifts towards species that have higher

133   calcite mass per individual combine with simple increases in test abundance (Fig. 1)

134   to enhance foraminifer-CaCO₃ fluxes and drive the observed patterns of species-

135   specific contributions to the carbonate counter pump (Fig 2c).

136

137   The continuous dataset enabled us to compare assemblage size and calcification

138   intensity (size-normalised weights; SNW)[21] of foraminifer species (Supplementary

139   Methods). No significant differences in assemblage size were observed in relation to

140   flux from iron-fertilized productivity (Supplementary Information 6). At the most

141   frequent size distributions, seasonal variability in SNWs was typically greater than

142   regional differences (Supplementary Information 6). Approximately two-fold ranges

143   in SNWs were observed for *G. bulloides* (~5-10 µg) and *N. pachyderma* (~2-4 µg) in

144   both +Fe and HNLC waters at different times of year (Supplementary Information 6)

145   and are possibly related to food supply, calcification depths and CO₂ concentrations.

146   The variability in SNWs appears to be of minor importance for enhanced CaCO₃

147   fluxes when compared to the increases in foraminifer test abundance (6-10 fold) and

148   shifts in species composition systematically linked to iron fertilisation.

149

150 The geographical location of the iron-fertilized Crozet bloom is of some significance

151 concerning the role of iron in promoting carbonate-counter pump effects. The

152 northernmost extent of the bloom is bound by the Subantarctic Front (Supplementary

153 Information 1); a boundary that marks a geochemical transition towards carbonate-

154 dominated production[22,23] (Supplementary Information 7). Temperature and salinity

155 data however indicate limited cross frontal exchange and influence of SAZ waters

156 within the bloom area[17]. To validate our dataset we analysed the geochemical

157 signatures of all published estimates of annual export in the Southern Ocean (Fig 3,

158 Supplementary Information 8). The POC:PIC ratio from HNLC waters south of

159 Crozet is comparable to other measurements in the same frontal region. However, the

160 combined geochemical signature of Si:PIC ratios >1 (diatom-dominated production)

161 and POC:PIC ratios <1 measured from the Crozet bloom is a uniquely consistent

162 feature of Polar Frontal Zone iron fertilisation. Strengthening of the carbonate

163 counter pump north of the Crozet Plateau thus occurs due to enhancement of CaCO$_3$

164 production and flux in response to iron fertilization, rather than a shift from silicate

165 dominated production characteristic of the Subantarctic Zone[22,23].

166

167 Although characteristic of the PFZ in general, the Si:PIC ratios in the HNLC area are

168 notably higher than those in the [+Fe] regime [Figure 3b]. The Si:PIC ratios at the

169 iron fertilized site [2.6±0.6 (n=3)] are significantly lower (P<0.005; two-tailed t-test)

170 than at the unfertilized HNLC site [11±2.2 (n=3)] (Supplementary Methods). The

171 iron-limited PFZ is characterised by the production of large heavily silicified diatom

172 species resistant to grazing and the resulting flux of their empty frustules[4].

173 Consequently biogenic SiO$_2$ fluxes are similar in both [+Fe] and HNLC

174 environments[4]. The observable decrease in deep-ocean POC:PIC ratios resulting

175 from iron fertilization in the PFZ appears to be primarily attributable to an increase in

176 PIC fluxes, relative to both POC and SiO_2

177

178 Heterotrophic $CaCO_3$ producers, notably foraminifer, are the dominant contributor

179 towards the carbonate counter pump (Fig 2b). The planktonic foraminifer

180 assemblages in our samples are typical species of sediments underlying the Sub

181 Antarctic Front (SAF) to Antarctic Polar Front (APF) during the late Pleistocene and

182 Holocene[18]. It is conceivable therefore that iron-fertilization north of the Polar Front

183 affected deep-ocean rain ratios in the manner proposed here over glacial-interglacial

184 cycles.

185

186 Changes in Southern Ocean organic carbon export upon iron fertilization have been

187 evoked to explain ~40 ppm of the CO_2 decline occurring over the last glacial

188 maximum[24,25]. Sedimentary records provide evidence that increases in nutrient

189 utilisation and export occurred in the Subantarctic Southern Ocean[26,27] and have been

190 linked to alteration of Aeolian iron supply[28,29]. Our data suggests that under a scenario

191 of glacial iron fertilization, strengthening of the carbonate counter pump in the

192 Subantarctic may have accompanied increases in organic carbon export.

193 Understanding the response of inorganic carbon flux to iron supply in this region is

194 therefore necessary to fully elucidate the role of the biological carbon pump in glacial

195 CO_2 drawdown. The dominant but variable response of foraminifer species to iron

196 fertilised production provides a strong rationale for quantifying $CaCO_3$ fluxes at the

197 species level. It is only with such detailed approaches that we can hope to advance

198 our understanding of the complex interactions between ocean biota and climate.

199

Method Summary

Sediment traps. Traps were McLane 21-cup time-series arrays deployed on bottom-tethered moorings[3,4]. The traps all functioned well in the water-column (supplementary information). Although unusual, the punctuated flux pattern at [HNLC]M6-S was identical to two additional annual flux profiles South of the Plateau (Supplementary Methods).

Foraminifer and pteropod CaCO₃: Samples were dry split according to the number of particles present (1/1 to 1/32, but generally 1/8 splits) with the exception of larger particles (>400μm), which were removed and weighed separately to avoid splitting uncertainty. Particle analyses were carried out with a fully automated incident light microscope system. Particles were manually classified and counted from the digital images and verified directly from the samples if necessary. Planktonic foraminifer test calcite mass is determined for each sampling interval of each sediment trap, and for each species, and test size fraction. Pteropods of the three species *Limacina inflata*, *Limacina retroversa*, and *Limacina helicina* were counted from the 63-100 µm and >100-µm size fractions or referred to as pteropod fragments if no classification was possible. Whole pteropod shells and fragments from the >100-µm size fraction were weighed with a microbalance to directly determine their CaCO₃ (aragonite) mass. To determine the aragonite weight of pteropods >400 µm the entire assemblage was weighed, i.e., all species and fragments together (Supplementary Methods).

Total and fine-fraction CaCO₃

Total particulate CaCO₃ was determined on freeze-dried sediments using a Carlo-Erba NA-1500 elemental analyser. Inorganic carbon was determined following the removal organic carbon by direct acidification and converted to CaCO₃. Coccolithophore-CaCO₃ fluxes were estimated from the determination of fine-

225   fraction carbonate weights in the <63 μm and 63-20 μm fractions[29]. A 1/80 aliquot

226   was wet-sieved over a 20μm mesh and the two size-fractions filtered on 0.4

227   polycarbonate membranes. The filters and particulate material were leached in 10 ml

228   1% HNO_3 solution and calcium content of the samples determined by inductively

229   coupled plasma atomic emission spectroscopy (ICP-AES). Further details can be

230   found in Supplementary Methods.

231   **Carbon drawdown reduction:** Reduction of carbon dioxide drawdown was

232   calculated from the expression: $(1-\{[(FPOC_{WML})-(FPIC_{WML}*\psi)] / (FPOC_{WML})\})*100$,

233   where $FPOC_{WML}$ is POC flux at the winter mixed layer depth, $FPIC_{WML}$ are

234   particulate inorganic carbon fluxes calculated from foraminifer (>63 μm), pteropod

235   (>63 μm), coccolithophore (<20/20-63 μm) or total, $CaCO_3$ measurements, and ψ is

236   released CO_2:precipated carbonate ratio[12]. The $CaCO_3$ fluxes measured at the

237   sediment trap deployment depths of 2000-3195m were taken as a minimum estimate

238   of the $CaCO_3$ fluxes at the base of the winter mixed layer and converted into molar

239   inorganic carbon (PIC) fluxes. We determined ψ values based on the mixed layer

240   inventories of dissolved inorganic carbon and total alkalinity at the sediment trap

241   deployment locations (Supplementary Information 4). Particulate organic carbon

242   (POC) fluxes measured at the sediment trap deployment depth were normalised to the

243   base of the winter mixed layer (200m) using the expression : $F_d = F_{WML} (WML/d)^{-b}$,

244   where F_d is the flux at the sediment trap deployment depth, F_{WML} is the flux at the

245   winter mixed layer depth WML), d is the sediment trap deployment depth, and the

246   exponent b characterises the attenuation of flux with depth. Under the constant

247   remineralisation scenario a b-value of 0.85 was used for all three sites and for the

248   regionally variable scenario a b-value of 0.5 was used at M10[+Fe]-N and M5[+Fe]-

249   NE and a b-value of 1.3 at M6[HNLC]-S[30].

250   **Tables and Figure Captions**

251

252   **Figure 1 | Annual and seasonal inorganic carbon (CaCO₃) fluxes** (a) Annual

253   inorganic carbon fluxes of total, fine fraction(<20μm) coccolith, 20-63um,

254   foraminifer calcite and pteropod aragonite at the M10[+Fe]-N (352 days), M5[+Fe]-

255   NE (357 days), M6[-Fe]-S (363 days) sediment trap deployment locations

256   (Supplementary Information S1) (b-d) Seasonality of inorganic carbon fluxes in

257   foraminifera and pteropod catergories. Time-series fluxes (mmol m^{-2} int.$^{-1}$) in (b-d)

258   are integrated over the sediment trap cup sampling interval and centred on the interval

259   mid-point (Supplementary Information 3). Absence of bars corresponds to periods of

260   negligible mass flux. The sample cups in which foraminifer species analyses were

261   conducted account for 98-99% of total annual CaCO₃ fluxes (Supplementary

262   Information 3).

263

264   **Figure 2 | Impact of carbonate counter pump (CCP) and the contribution of**

265   **CaCO₃ fractions and foraminifer species in reducing deep-ocean CO₂ storage**.

266   (**a**) The reduction in deep-ocean CO₂ storage calculated from different

267   methodological estimates of POC export beyond the ventilation depth. Sediment trap

268   (Sed. Trap) estimates are annual deep-ocean POC fluxes extrapolated to regional

269   winter mixed layers[3,17] using either constant[3,28] or bloom/HNLC[29]-variable POC

270   attenuation co-efficient (Methods). Dissolved inorganic carbon estimates are based on

271   seasonal drawdown[30] and mixed layer remineralisation rates of 90% or 75%

272   (Supplementary Information 4). ^{234}Th are based on seasonal estimates extrapolated to

273   150 and 200m^3. The relative contributions of CaCO₃ fractions (b) and foraminifer

274   species within foraminifer fraction (c) to the carbonate counter pump.

275

276   **Figure 3 | Comparison of particulate geochemical signatures comprising**

277   **Southern Ocean Flux.** (a) Map showing sediment trap deployment locations in

278   relation to Southern Ocean Fronts and sea-ice extent (Supplementary Information 8).

279   SAF- Subantarctic Front, PF-Polar Front, SAZ-Subantarctic Zone, PFZ-Polar Frontal

280   Zone, POOZ-Permanently Open Ocean Zone, SIZ-Seasonal Ice Zone (b) POC:PIC

281   ratios of annual flux compared to Si:PIC ratios. Dashed lines mark unity. PFZ[+Fe]

282   and PFZ[HNLC] correspond to the M10[+Fe]-N;M5[+Fe]-NE and (357 days),

283   M6[HNLC]-S sediment trap fluxes around the Crozet Plateau (this study).

284

285

286   **References**

287   1. Boyd, P.W. *et al*. A mesoscale phytoplankton bloom in the polar Southern

288   Ocean stimulated by iron fertilization. *Nature* **407**, 695-702 (2000).

289   2. Blain, S. *et al*. Effect of natural iron fertilization on carbon sequestration in the

290   Southern Ocean. *Nature* **446**, 1070-1074 (2007).

291   3. Pollard, R.T. *et al*. Southern Ocean deep-water carbon export enhanced by

292   natural iron fertilization. *Nature* **457**, 577-580 (2009).

293   4. Salter, I. *et al*. Diatom resting spore ecology drives enhanced carbon export

294   from a naturally iron-fertilized bloom in the Southern Ocean. *Global*

295   *Biogeochem. Cy.* **26**, GB1014 (2012).

296   5. Smetacek, V. *et al*. Deep carbon export from a Southern Ocean iron-fertilized

297   diatom bloom. *Nature* **487**, 313-319 (2012).

298   6. Martin, J.H. Glacial-interglacial CO₂ change: the iron hypothesis.

299   *Paleoceanography* **5**, 1-13 (1990).

300   7. Sigman, D.M. & Boyle, E.A. Glacial/interglacial variations in atmospheric

301   carbon dioxide. *Nature* **407**, 859-869 (2000).

302   8. Buesseler, K.O. & and Boyd, P.W. Will ocean fertilization work? *Science* **300**,

303   67-68 (2003).

304   9. Antia, A.N. *et al*. Basin-wide particulate carbon flux in the Atlantic Ocean:

305   Regional export patterns and potential for atmospheric CO_2 sequestration.

306   *Global Biogeochem. Cy.* **15**, 845-862 (2001).

307   10. Volk, T. & Hoffert M.I. In The Carbon Cycle and Atmospheric CO_2: Natural

308   Variations Arcana to Present. *Geophys. Monogr. Ser.* Eds Sunquist E.T. &

309   Broeker W.S. (Washington, DC) **32**, 99-111 (1985).

310   11. Heinze, C., Maier-Reimer, E., Winn, K. Glacial pCO_2 reduction by the world

311   ocean : Experiments with the Hamburg carbon cycle model.

312   Paleoceanography **6**, 395-430 (1991).

313   12. Frankingnoulle, M., Canon, C., Gattuso, J.P. Marine calcification as a source

314   of carbon dioxide : Positive feedback of increasing atmospheric CO_2. *Limnol.*

315   *Oceanogr.* **39**, 458-462 (1994).

316   13. Zeebe, R.E. History of Seawater Carbonate Chemistry, Atmospheric CO_2, and

317   Ocean Acidification. *Ann. Rev. Ear. Plan. Sci.* **40**, 141-165 (2012).

318   14. King, A.L. & Howard, W.R. $\partial^{18}O$ seasonality of planktonic foraminifera from

319   Southern Ocean sediment traps : latitudinal gradients and implications for

320   paleoclimate reconstructions. *Mar. Micropaleontol.* **56**, 1-24 (2005).

321   15. Schiebel, R. Planktic foraminiferal sedimentation and the marine calcite

322   budget. *Global Biogeochem. Cy.* **16**, 1065, (2002).

323   16. Wolff, G.A. *et al*. The effects of Natural Iron Fertilization on Deep Sea

324   Ecology: The Crozet Plateau, Southern Indian Ocean. PLoS ONE 6(6) e20697

325   (2011).

326   17. Venables, H.J., Pollard, R.T., Popova E.E. Physical conditions controlling the

327   development of a regular phytoplankton bloom north of the Crozet Plateau,

328   Southern Ocean. *Deep-Sea Res. Pt II* **54**, 1949-1965 (2007).

329   18. Howard, W.R. *et al*. Distribution, abundance and seasonal flux of pteropods

330   in the Sub-Antarctic Zone. *Deep-Sea Res. Pt II* **58**, 2293-2300 (2011).

331   19. Roberts, D. *et al*. Interannual pteropod variability in sediment traps deployed

332   above and below the aragonite saturation horizon in the Sub-Antarctic

333   Southern Ocean. *Polar Biol*. **34**, 1739-1750 (2011).

334   20. Schiebel, R. *et al*. Planktonic foraminiferal dissolution in the twilight zone.

335   *Deep-Sea Res. Pt II* **54**, 676-686 (2007).

336   21. Moy, A.D. *et al*. Reduced calcification in modern Southern Ocean planktonic

337   foraminifera. *Nat. Geosci.* **2**, 276-280 (2009).

338   22. Honjo, S. *et al*. Particle fluxes to the interior of the Southern Ocean in the

339   Western Pacific sector along 170°W. *Deep-Sea Res. Pt II* **47,** 3521-3548

340   (2000).

341   23. Trull, T. *et al*. Moored sediment trap measurements of carbon export in the

342   Subantarctic and Polar Frontal Zones of the Southern Ocean, south of

343   Australia. *J. Geophys. Res*. **106**, 31489-31509 (2001).

344   24. Watson, A. J. *et al*. Effect of iron supply on Southern Ocean CO_2 uptake and

345   implications for atmospheric CO_2. Nature **407**, 730–733 (2000)

346   25. Sigman, D.M. *et al*. The polar ocean and glacial cycles in atmospheric CO_2

347   concentration. *Nature* **466**, 47-55 (2010).

348   26. Robinson, R. S. *et al*. Diatom-bound ^{15}N/^{14}N: new support for enhanced

349   nutrient consumption in the ice age subantarctic. *Paleoceanography* **20**,

350   PA3003, (2005)

351   27. Kohfeld, K. E. *et al*. Role of marine biology in glacial-interglacial CO_2 cycles.

352   *Science* **308**, 74–78 (2005).

353   28. Mahowald, N.M. *et al*. Change in atmospheric mineral aerosols in response to

354   climate: Last glacial period, preindustrial, modern and doubled carbon dioxide

355   climates. *J. Geophys. Res* **111**, D10202 (2006).

356   29. Martínez-Garcia, A. *et al*. Iron fertilization of the Subantarctic ocean during

357   the last ice age. *Science* **343**, 1347-1350 (2014).

358   30. Buesseler, K.O. *et al*. Revisiting carbon flux through the ocean's twilight

359   zone. *Science* **316**, 567-570 (2005).

360

361   **Supplementary Information** is linked to the online version of the paper at

362   www.nature.com/nature.

363

372

387

388 **Table 1. Excess fluxes at [Fe] and [HNLC] sites**

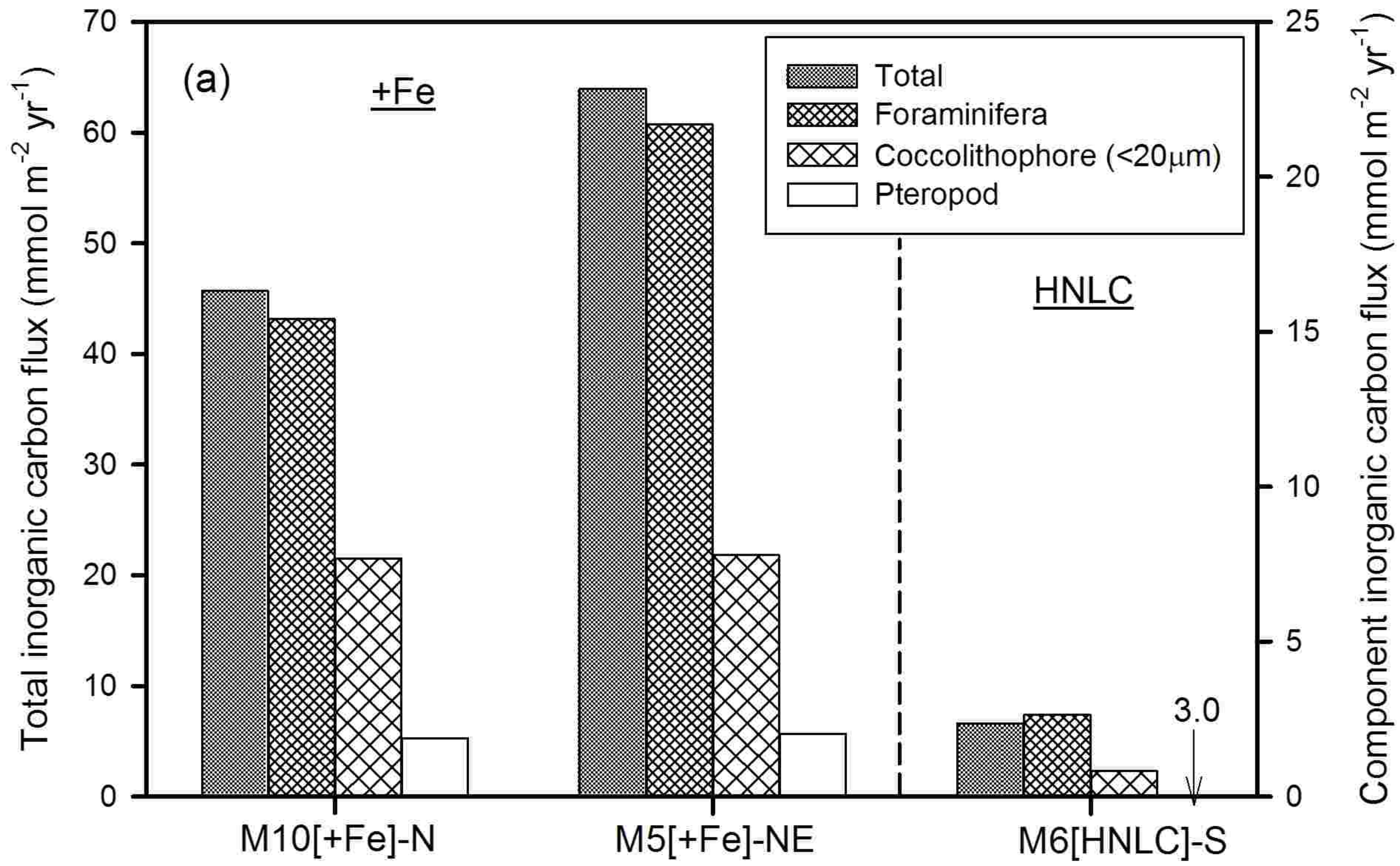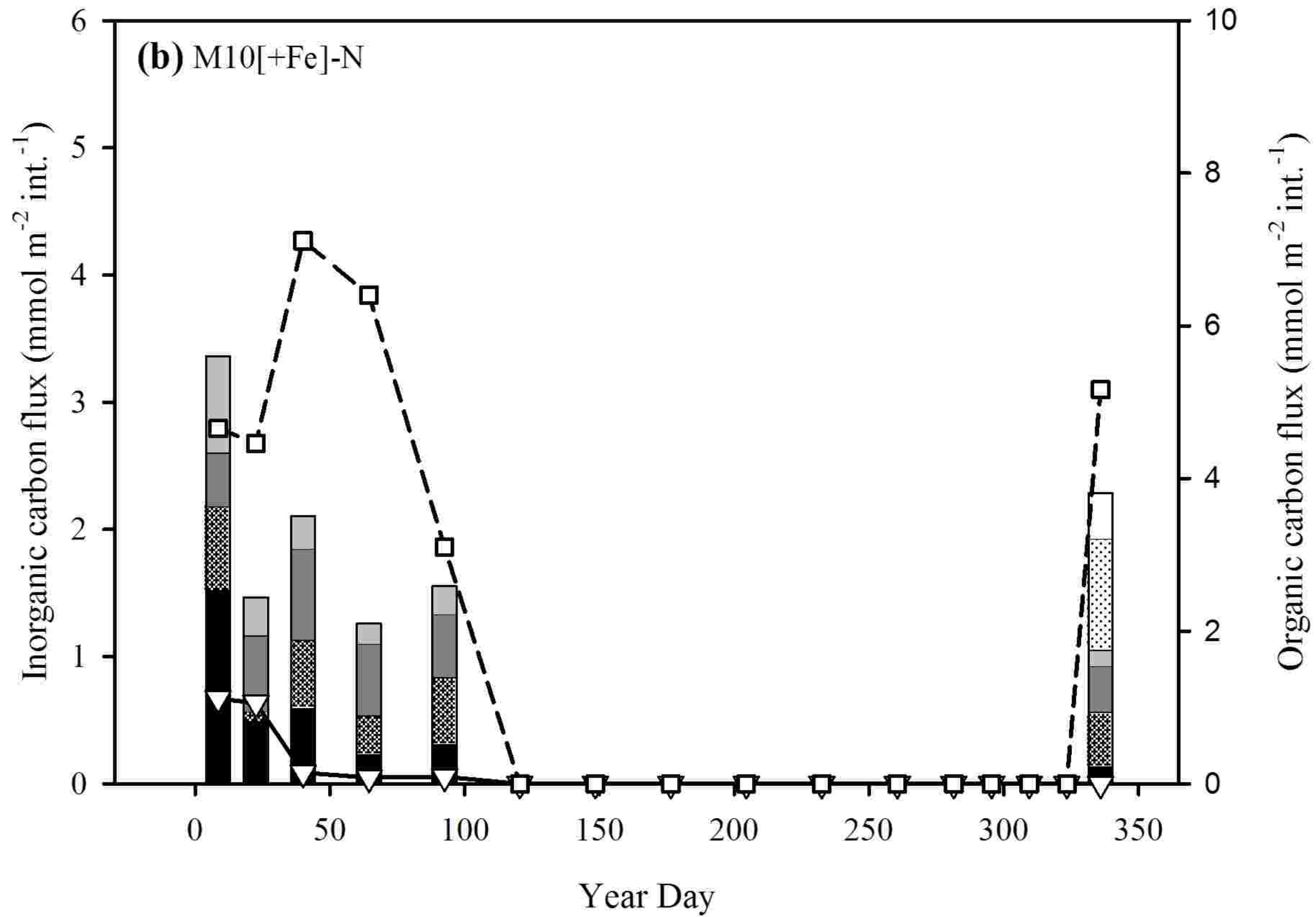|	C_{org} Total	C_{inorg} Total	C_{inorg} Foram	C_{inorg} Pteropod	C_{inorg} <20 μm
Excess Fluxes[1],*	24-27	39-57	13-19	1.8-2.0	6.9-7.0
Increase[2],*	~3	7-10	6-8	63-68	~9

389

390 [1]Excess fluxes in mmol m^{-2} yr^{-1} calculated as [+Fe] – [HNLC] annual fluxes
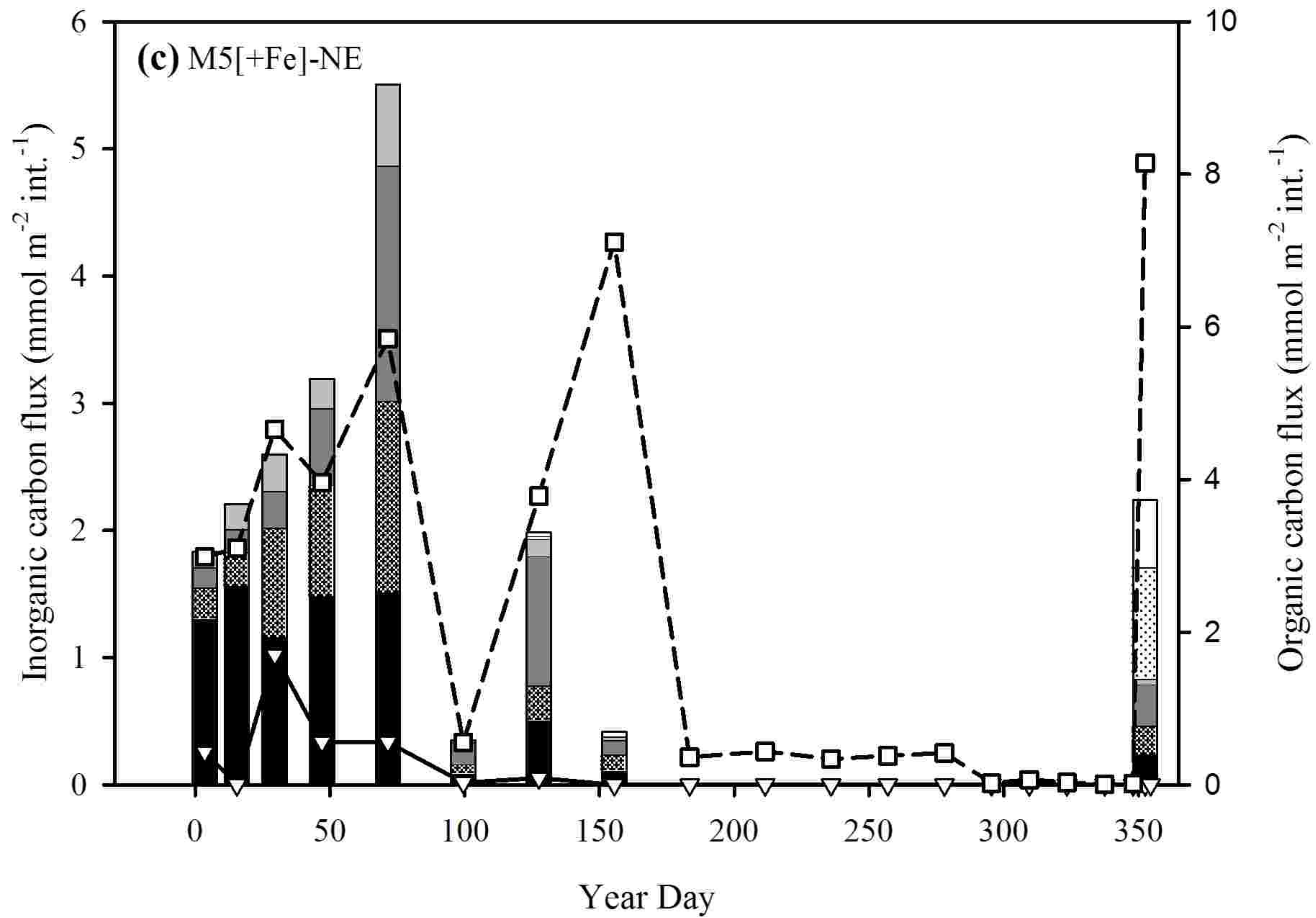
391 [2]Factoral increase, calculated as [+Fe] / [HNLC]

392 *Calculated as difference between [+Fe] and [HNLC] annual fluxes
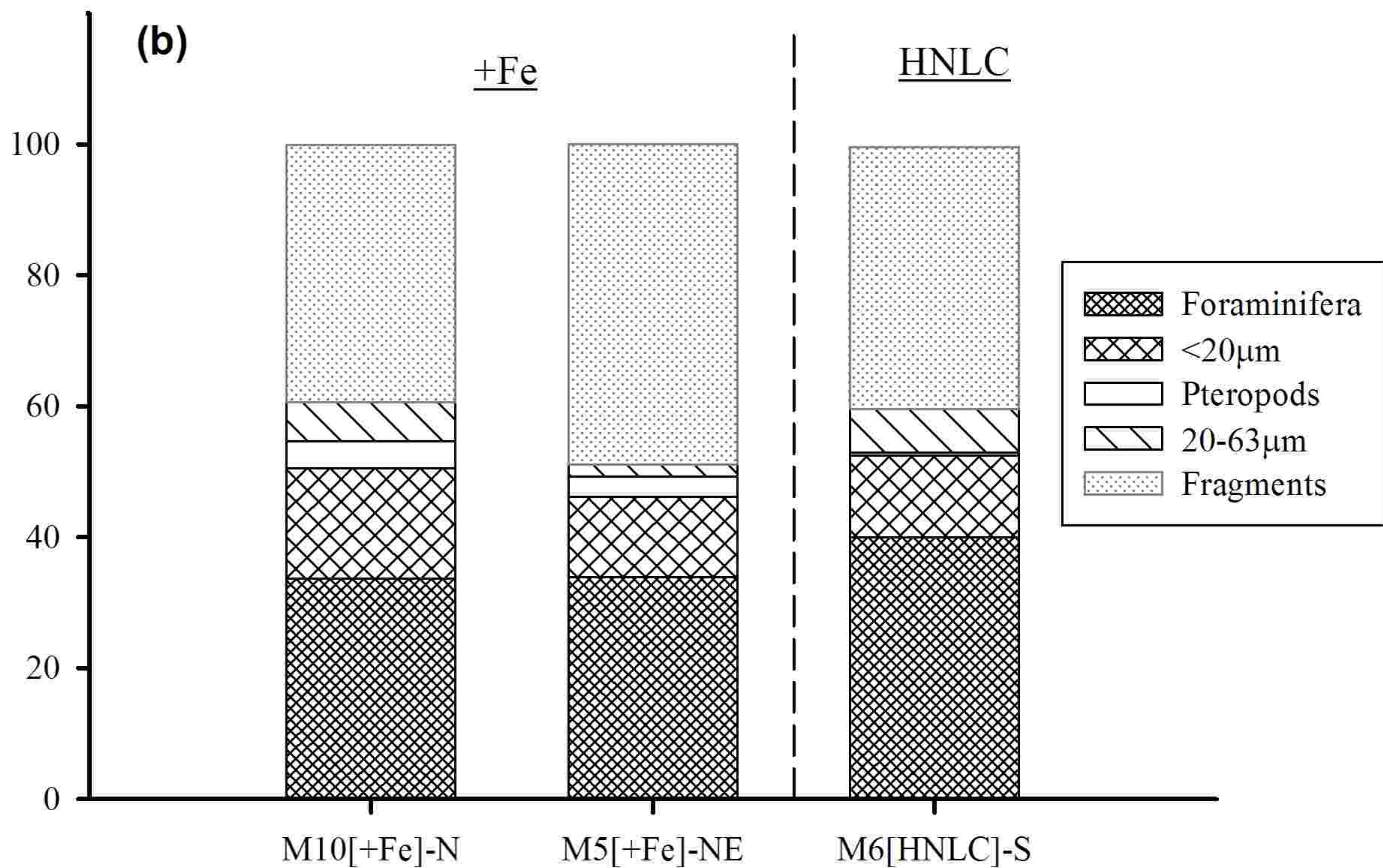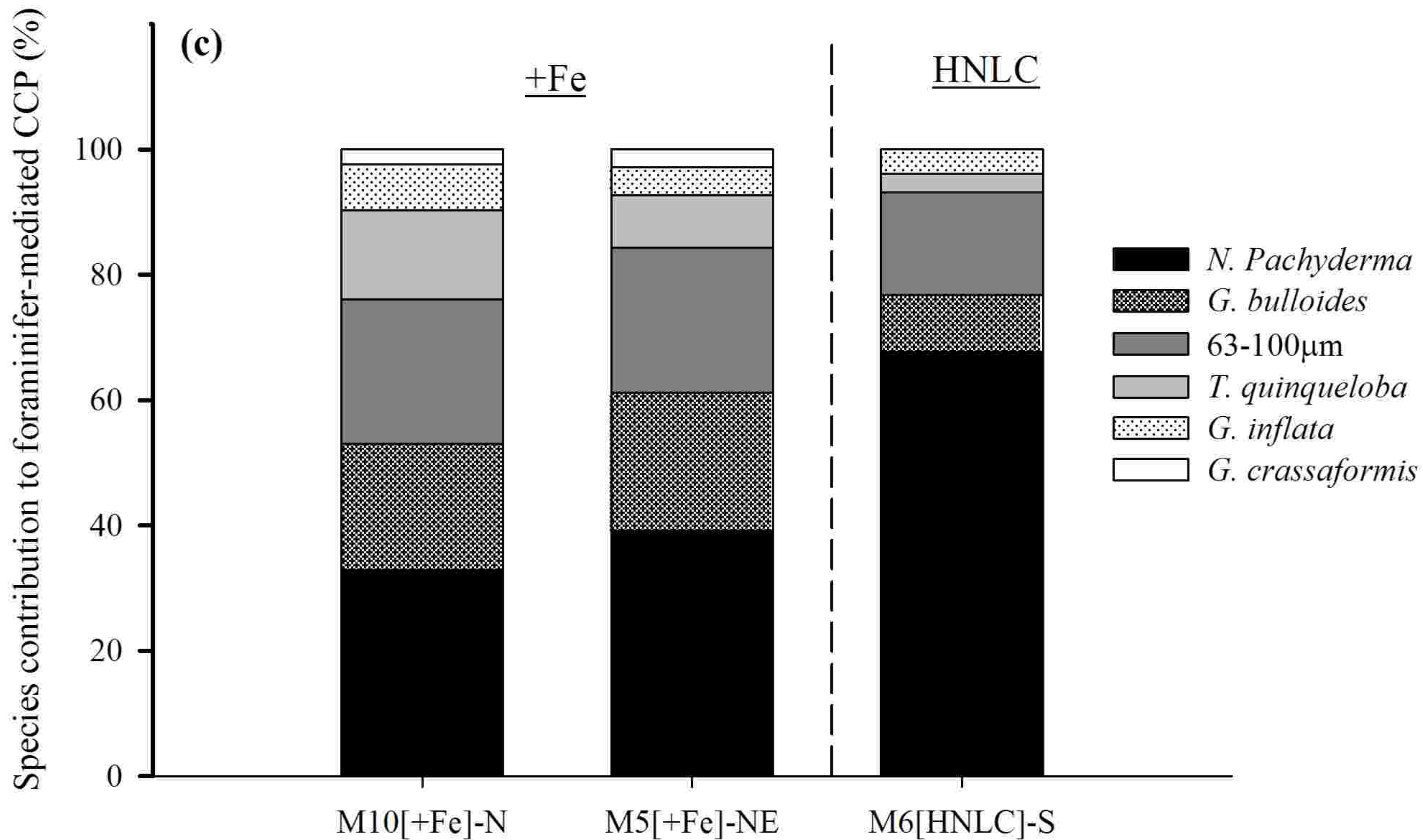
393

394

(a)

(b) M10[+Fe]-N

(c) M5[+Fe]-NE
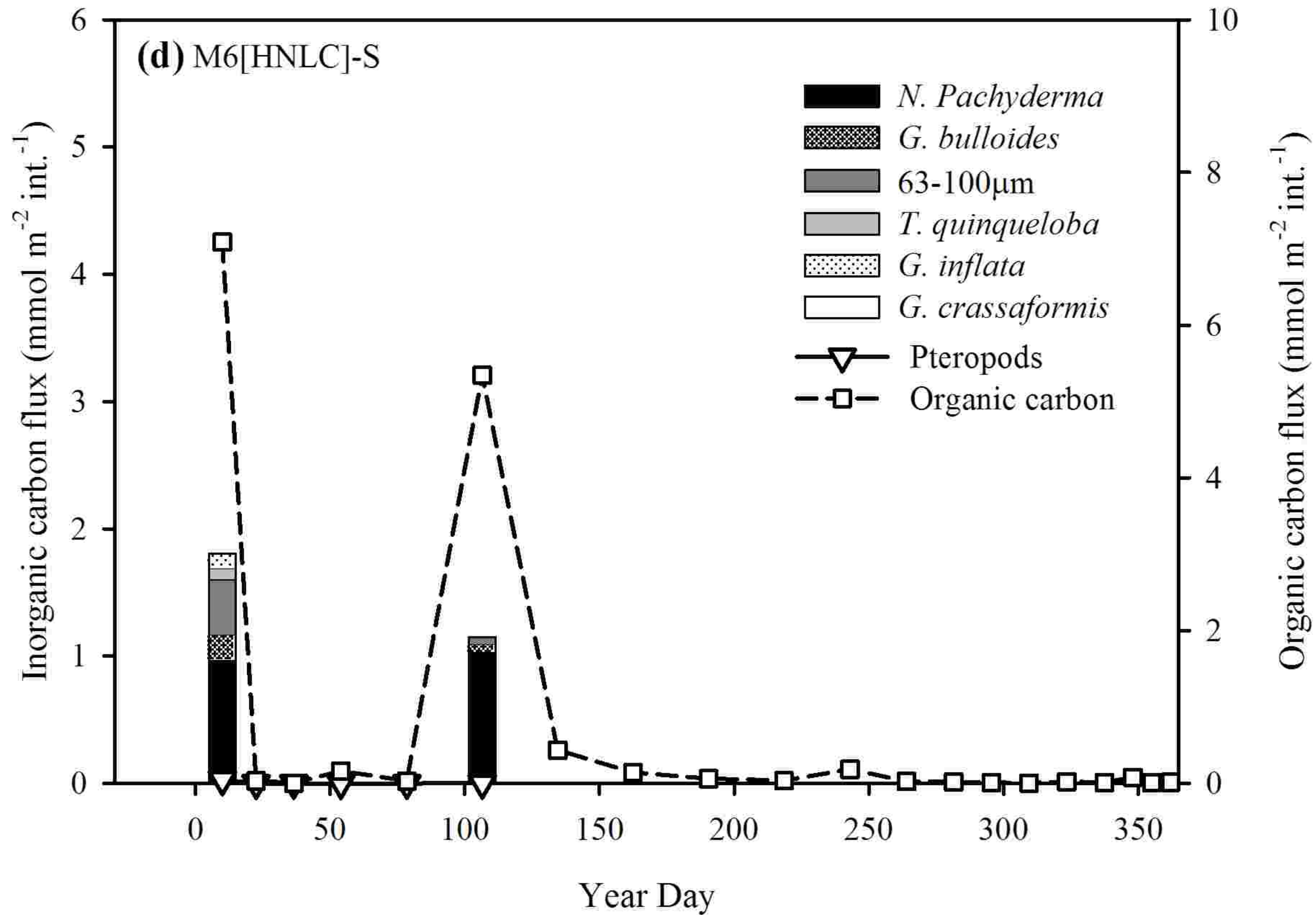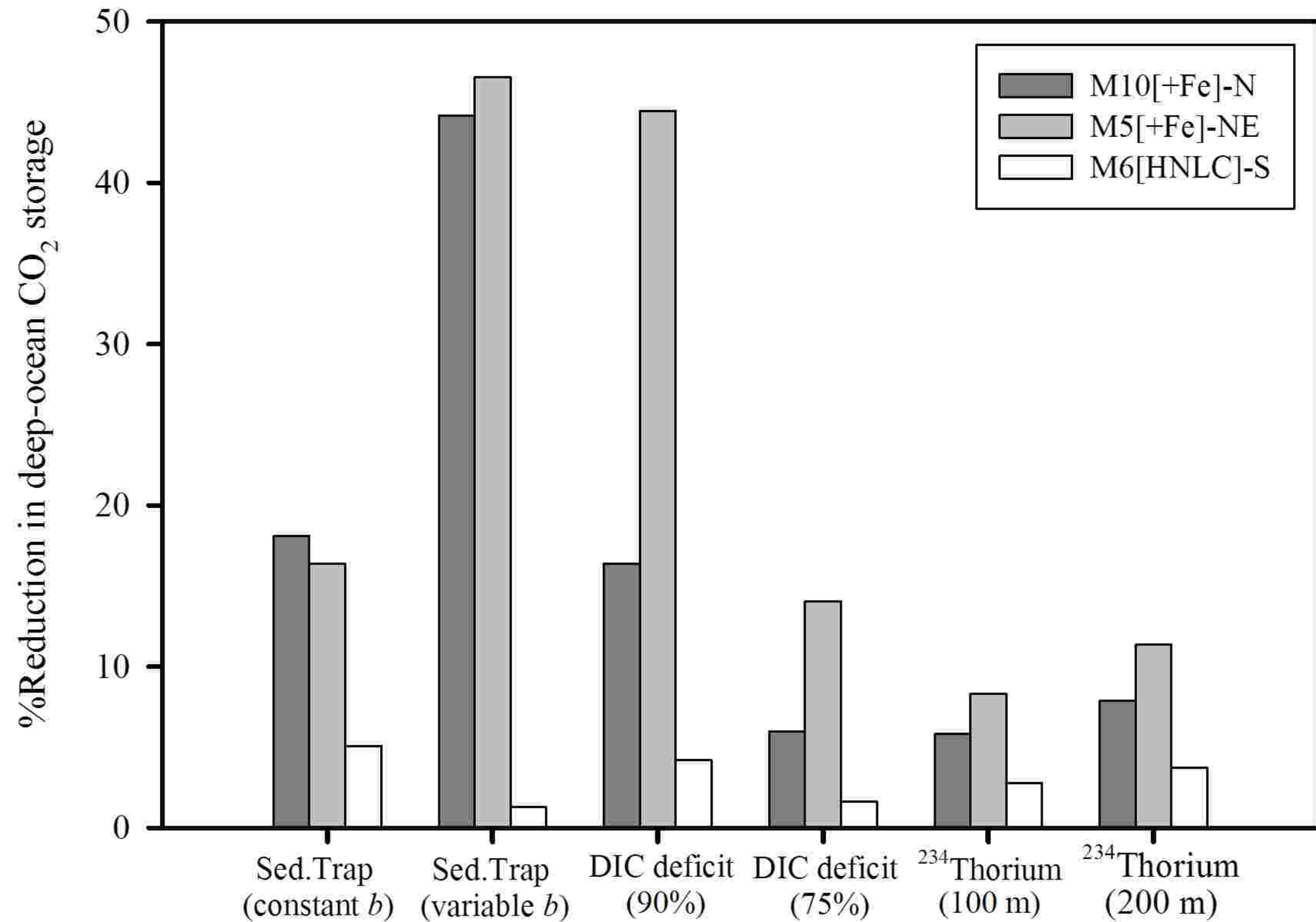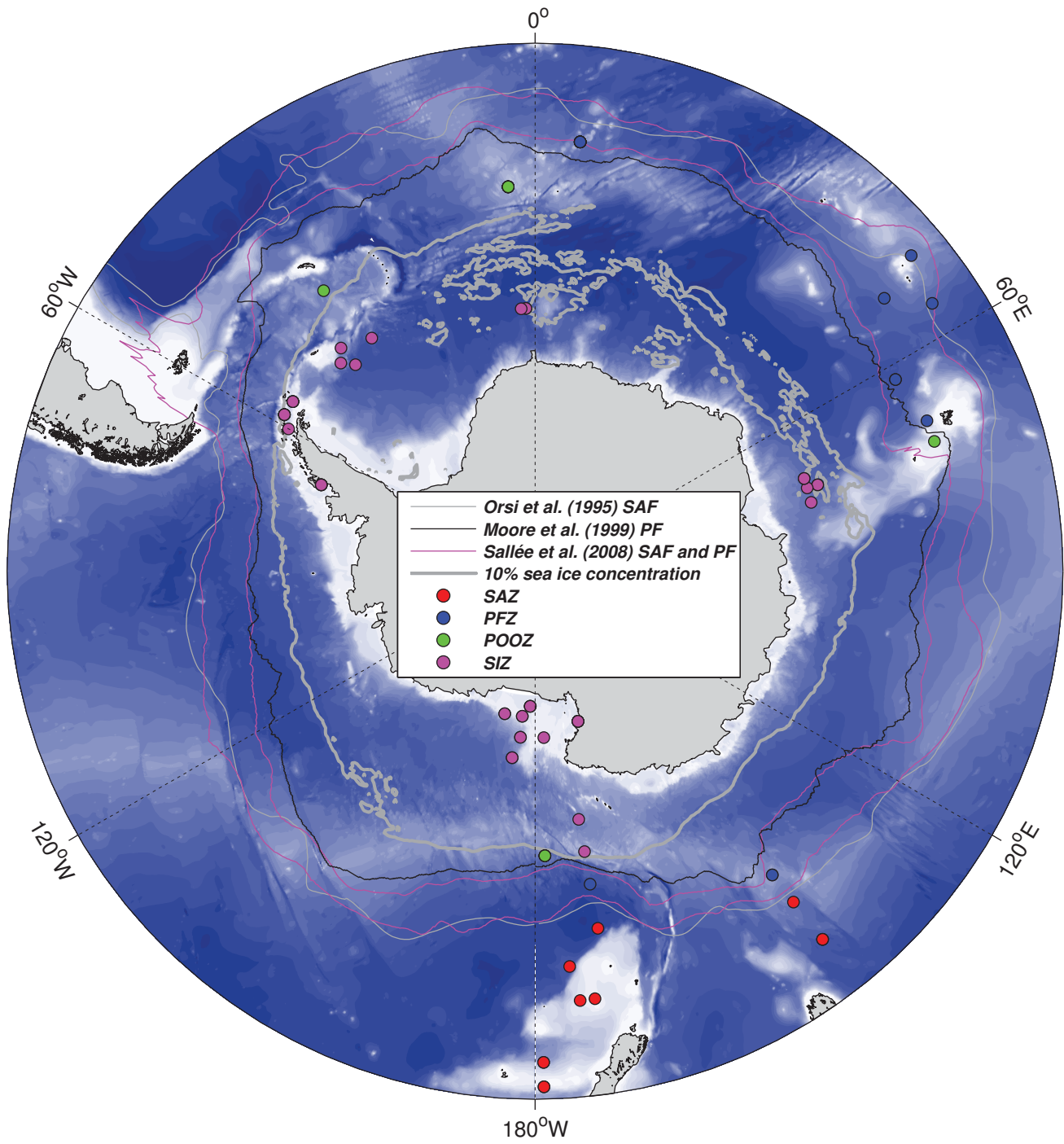
——	*Orsi et al. (1995) SAF*
——	*Moore et al. (1999) PF*
——	*Sallée et al. (2008) SAF and PF*
——	*10% sea ice concentration*
●	*SAZ*
●	*PFZ*
●	*POOZ*
●	*SIZ*